

Optimal efficiency of quantum transport in structured disordered systems with applications to light-harvesting complexes

G G Giusteri^{1,2}, G L Celardo¹ and F Borgonovi¹

¹Dipartimento di Matematica e Fisica and Interdisciplinary Laboratories for Advanced Materials Physics, Università Cattolica del Sacro Cuore, via Musei 41, I-25121 Brescia, Italy *and* Istituto Nazionale di Fisica Nucleare, Sezione di Pavia, via Bassi 6, I-27100, Pavia, Italy

²International Research Center on Mathematics & Mechanics of Complex Systems, via XIX marzo 1 I-04012 Cisterna di Latina, Italy

E-mail: giulio.giusteri@unicatt.it

Abstract. Disordered quantum networks, as those describing light-harvesting complexes, are often characterized by the presence of antenna structures where the light is captured and inner structures (reaction centers) where the excitation is transferred. Antennae often display distinguished coherent features: their eigenstates can be separated, with respect to the transfer of excitation, in the two classes of superradiant and subradiant states. Both are important to optimize transfer efficiency. In absence of disorder superradiant states have an enhanced coupling strength to the RC, while subradiant ones are basically decoupled from it. Disorder induces a coupling between subradiant and superradiant states, thus creating an indirect coupling to the RC. We consider the problem of finding the maximal excitation transfer efficiency as a function of the RC energy and the disorder strength, first in a paradigmatic three-level system and then in a realistic model for the light-harvesting complex of purple bacteria. Specifically, we focus on the case in which the excitation is initially on a subradiant state, showing that the optimal disorder is of the order of the superradiant coupling. We also determine the optimal detuning between the initial state and the RC energy. We show that the efficiency remains high around the optimal detuning in a large energy window, proportional to the superradiant coupling. This allows for the simultaneous optimization of excitation transfer from several initial states with different optimal detuning.

PACS numbers: 71.35.-y, 05.60.Gg

Keywords: quantum transport in disordered systems; open quantum systems; light-harvesting complexes.

1. Introduction

Photosynthetic bacteria utilize antenna complexes to capture photons and convert the energy of the short-lived electronic excitation in a more stable form, such as chemical bonds. After absorption, the energy is transferred to a complex, called reaction center (RC), where it initiates electron transfer, resulting in a membrane potential. This very efficient transfer occurs on a time-scale of few hundreds of picoseconds and on a length-scale of few nanometers, so that coherent quantum dynamics can enter the play, as recent experiments seem to prove [1]. Quantum coherence can enhance transport efficiency inducing Supertransfer and Superradiance in light-harvesting complexes [2, 3, 4]. On the other hand, quantum coherence can also be detrimental to transport, as Anderson localization [5] and the presence of trapping-free subspaces [6] show.

Superradiance [7, 8, 9], as viewed in the context of both optical fluorescence [10, 11, 12] and quantum transport in open systems [13, 2, 14, 15, 16], is not solely a many-body effect. Single-excitation superradiance is a prominent example of genuinely quantum cooperative effect [17], relevant in natural complexes, which operate in the single excitation regime since solar light is very dilute.

Natural complexes are subject to a noisy environment with different correlation time-scales (if compared to the excitonic transport time): (i) short-time correlations, giving rise to dephasing (homogeneous broadening, as considered e.g. in [18, 19, 20, 21]) and (ii) long-time correlations, producing on-site static disorder (inhomogeneous broadening, as considered e.g. in [22, 23]). The role of environmental noise is twofold: on one hand, it can help transport since it destroys the detrimental coherent effects, leading to noise-enhanced energy transfer, i.e. the existence of a maximal efficiency at some intermediate noise strength, as found in the last decade by various groups [24, 25, 19, 20, 6, 26, 18, 27, 28, 29, 21, 30]. On the other hand, it can suppress the beneficial coherences leading to a quenching of Supertransfer [15]. It is thus essential to consider this non-trivial interplay when dealing with realistic light-harvesting complexes, as it will be shown below.

The typical structure of bacterial photosynthetic complexes displays a RC placed at the center of the light-harvesting complex I (LHI), with the chromophores arranged on a ring and surrounded by other ring structures (called LHII) acting as peripheral antennae. The LHI-RC structure describing light-harvesting complexes produces a distinguished feature: the eigenstates of the peripheral ring structure can be separated into two classes, superradiant and subradiant states, with respect to the transfer of excitation towards the RC. In absence of disorder, the superradiant states are coupled to the RC with a coupling amplitude proportional to \sqrt{N} , where N is the number of chromophores in the ring, while subradiant states are basically decoupled from the RC. In presence of disorder, the subradiant states can be coupled to the superradiant ones and, as a consequence, only indirectly coupled to the RC states. Note that the subradiant subspace, previously studied by the authors [15], has been also analyzed in the literature under the name of trapping-free subspace [6].

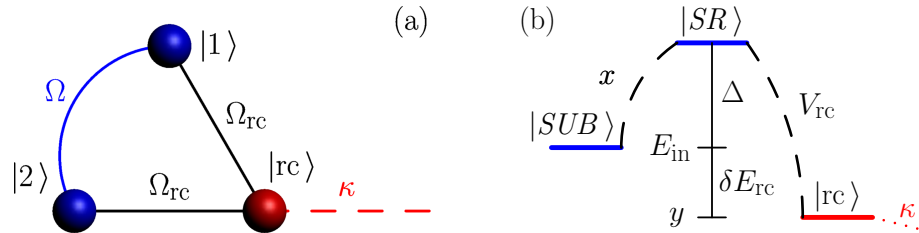


Figure 1. In panel (a) the trimer model is shown in the site basis: two sites connected with the RC with equal coupling Ω_{rc} and between them with coupling Ω . In panel (b) the trimer model is shown in the superradiant-subradiant-RC basis, see text.

Here we want to discuss the optimization of excitation transfer efficiency from peripheral states in networks displaying the Ring-RC structure, with particular reference to subradiant initial states. Indeed, since disorder is only detrimental for the superradiant state, we expect that the optimal condition will be mainly determined by the behavior of subradiant states. Nevertheless, the role of superradiant states is very important [15] and it will be the subject of future investigations.

Even if in natural systems the role played by dephasing is crucial, here we will focus only on the interplay of static disorder and energy landscape (energy detuning between the initial state and the RC) on transport efficiency.

To pursue our goal, we consider in section 2 a paradigmatic model: a trimer displaying a superradiant and a subradiant state, on which the excitation is initialized, and an acceptor state (the RC), where the excitation can be trapped, see figure 1. In absence of disorder, while the subradiant state is decoupled from the RC, the superradiant state has an enhanced coupling V_{rc} to the RC. We discuss the maximization of the average (over disorder) transfer efficiency with respect to both the detuning δE_{rc} between initial subradiant state and RC and the strength W of disorder. We have found two different regimes depending on V_{rc} and the energy gap Δ between the subradiant and superradiant states. While the optimal noise is always of the order of V_{rc} , the optimal detuning occurs at resonance with the initial energy, $\delta E_{rc} = 0$, only for $V_{rc} > \Delta$. Another optimal detuning, $\delta E_{rc} = V_{rc}^2/\Delta$, should be used in the case $V_{rc} \lesssim \Delta$.

In section 3 we show the relevance of our findings in a more realistic model by analyzing the LHI-RC complex of purple bacteria as presented in [31]. After a reduction of the whole system to simpler systems capable to describe its main features, we prove that the optimal conditions for the excitation transfer from a room-temperature Gibbs distribution of ring states can be estimated by applying our analysis. The optimal disorder strength we find falls within the estimated range of natural disorder strength. We conclude the paper (section 4) with a summary of the main results and of future research directions.

2. The trimer model

Many transport properties of systems displaying the Ring-RC structure can be understood from the analysis of the simplest ring, i.e. two coupled sites, connected with a central site representing the RC, as depicted in figure 1a. The Hamiltonian (in site-basis) for such trimer model can be written in matrix form as follows:

$$\begin{pmatrix} E_1 - i\Gamma_{\text{fl}}/2 & \Omega & \Omega_{\text{rc}} \\ \Omega & E_2 - i\Gamma_{\text{fl}}/2 & \Omega_{\text{rc}} \\ \Omega_{\text{rc}} & \Omega_{\text{rc}} & E_{\text{rc}} - i(\Gamma_{\text{fl}} + \kappa)/2 \end{pmatrix} \quad (1)$$

where the action of the environment (static disorder) has been taken into account by choosing the energy levels E_k , $k = 1, 2$, as Gaussian random numbers with mean zero and variance W^2 , and no disorder has been added to the RC site.

The loss of excitation through the RC has been described by the non-Hermitian term $-i\kappa/2$. Throughout the whole paper, κ is assumed to be small with respect to the other coupling parameters. This choice is consistent with the realistic photosynthetic model which will be considered in the next section. In order to make a close comparison with realistic systems and following a standard procedure [2, 3, 15, 14, 16], we also introduced the diagonal non-Hermitian terms $-i\Gamma_{\text{fl}}/2$, with fluorescence constant Γ_{fl} much smaller than any other energy scale ($\Omega, \Omega_{\text{rc}}, W, \kappa$), which represent the loss of excitation from each site due to recombination.

It is convenient to move from the site-basis to the subradiant-superradiant-RC basis, by defining the states

$$\begin{aligned} |SUB\rangle &= \frac{1}{\sqrt{2}} (|1\rangle - |2\rangle), \\ |SR\rangle &= \frac{1}{\sqrt{2}} (|1\rangle + |2\rangle), \end{aligned}$$

from which the new Hamiltonian H easily follows, see also figure 1b:

$$H = \begin{pmatrix} -\Omega - i\Gamma_{\text{fl}}/2 & x & 0 \\ x & \Omega - i\Gamma_{\text{fl}}/2 & \sqrt{2}\Omega_{\text{rc}} \\ 0 & \sqrt{2}\Omega_{\text{rc}} & y - i(\Gamma_{\text{fl}} + \kappa)/2 \end{pmatrix}, \quad (2)$$

where the two Gaussian random variables $x = (E_1 - E_2)/2$ and $y = E_{\text{rc}} - (E_1 + E_2)/2$ have been introduced and are such that

$$\langle x \rangle = 0, \quad \langle y \rangle = E_{\text{rc}}, \quad \langle x^2 \rangle = \langle y^2 \rangle - E_{\text{rc}}^2 = W^2/2.$$

In this basis, the coupling between the subradiant state and the RC vanishes, whereas the coupling between the superradiant state and the RC is enhanced and it is given by the matrix element $V_{\text{rc}} = \sqrt{2}\Omega_{\text{rc}}$. Note that in a ring of N sites, the superradiant coupling V_{rc} typically scales as \sqrt{N} . The structure of the Hamiltonian, depicted in figure 1b, implies that the excitation transfer from the subradiant state to the RC can only be mediated by the superradiant state, through the random coupling x .

Since we are interested in modeling light-harvesting complexes, a most relevant quantity is the efficiency, at the time t , of energy transfer from the system into the RC. Given an initial state $|\Psi_{\text{in}}\rangle$, it is defined as

$$\eta_{\Psi_{\text{in}}}(t) = \left\langle \kappa \int_0^t |\langle \text{RC} | e^{-\frac{i}{\hbar} H \tau} |\Psi_{\text{in}}\rangle|^2 d\tau \right\rangle_W, \quad (3)$$

and it represents the probability of escaping out of the system up to the time t . In the above definition the brackets $\langle \dots \rangle_W$ indicate the average over disorder.

In numerical simulations we always consider the efficiency at a time $t \gtrsim \hbar/\Gamma_{\text{fl}}$. Note that the efficiency strongly depends on the time t at which it is computed for $t < \hbar/\Gamma_{\text{fl}}$, while it reaches a stable asymptotic value η^∞ for $t \gtrsim \hbar/\Gamma_{\text{fl}}$, thus motivating our choice. As $\Gamma_{\text{fl}} \rightarrow 0$, the asymptotic value of the efficiency is $\eta^\infty = 1$ for any choice of parameters. Hereafter we will measure energies in cm^{-1} and times in ps, that corresponds to setting $1/\hbar \simeq 0.06\pi \text{ cm/ps}$.

It is clear from (3) that the energy transfer efficiency is strongly dependent upon the initial state, a feature also studied in [23]. Indeed, if we start from the superradiant state we are in a situation in which there is an enhanced direct coupling to the RC at zero disorder. Thus, one might think that the best situation occurs when the excitation is on the superradiant state set at resonance with the energy of the RC. In this situation disorder is only detrimental to transport, since it tends to destroy the superradiant coupling [10, 15] and it moves the system out of resonance. On the other side, the excitation in natural complexes is usually spread also on subradiant states, due to the presence of a thermal bath. Since a subradiant state is not directly coupled to the RC, it is only through the action of disorder that the excitation can be transferred from the initial state to the RC (i.e. for $W = 0$, we have $\eta = 0$).

We will focus our attention on this non-trivial case (see figure 1b), in which an initial excitation is on the subradiant state at energy $E_{\text{in}} = -\Omega$, coupled via x to the superradiant state at energy $E_{\text{sr}} = \Omega = E_{\text{in}} + \Delta$, which is further coupled to the RC with tunnelling amplitude $V_{\text{rc}} = \sqrt{2}\Omega_{\text{rc}}$. Our aim is to find the system configuration which maximizes the average transfer efficiency at $t \gtrsim \hbar/\Gamma_{\text{fl}}$. Fixing the energy gap $\Delta = 2\Omega$ between the superradiant and the subradiant states and the superradiant-RC coupling V_{rc} , and assuming κ and Γ_{fl} to be perturbative quantities, we are left with two independent parameters to be tuned to achieve the maximal efficiency: the subradiant-RC detuning $\delta E_{\text{rc}} = E_{\text{rc}} - E_{\text{in}}$ and the strength W of the random coupling x .

To pursue our goal we will first analyze a fully deterministic model obtained replacing the stochastic terms x and y in equation (2) with deterministic parameters as follows:

$$H^{\text{det}} = \begin{pmatrix} E_{\text{in}} - i\Gamma_{\text{fl}}/2 & X & 0 \\ X & E_{\text{in}} + \Delta - i\Gamma_{\text{fl}}/2 & V_{\text{rc}} \\ 0 & V_{\text{rc}} & E_{\text{rc}} - i(\Gamma_{\text{fl}} + \kappa)/2 \end{pmatrix}. \quad (4)$$

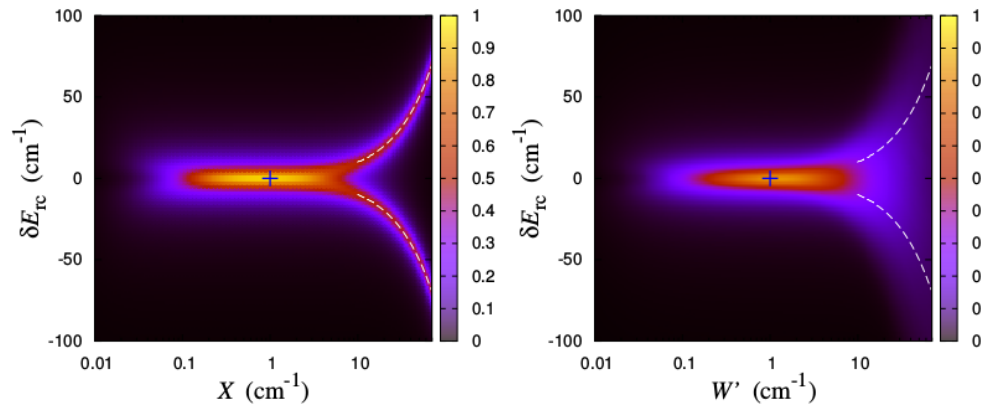


Figure 2. Average transfer efficiency η at fluorescence time $t_{\text{fl}} = \hbar/\Gamma_{\text{fl}}$, computed starting from the subradiant state $|SUB\rangle$, plotted in the left panel as a function of the subradiant-RC detuning δE_{rc} and of the deterministic subradiant-superradiant coupling X , and in the right panel as a function of δE_{rc} and of the rescaled disorder strength $W' = W/\sqrt{2}$. The blue cross indicates the estimate (5) for the optimal transfer conditions. The dashed curves indicate the resonances determined in (8). The value of the parameters are $\Delta = 0 \text{ cm}^{-1}$, $V_{\text{rc}} = 1 \text{ cm}^{-1}$, $\kappa = 0.01 \text{ cm}^{-1}$, and $\Gamma_{\text{fl}} = 10^{-4} \text{ cm}^{-1}$.

In particular, we will discuss which pair $(\delta E_{\text{rc}}^{\text{opt}}, X_{\text{opt}})$ of values of the subradiant-RC detuning and coupling strength produce the maximal efficiency. Subsequently, we will investigate how disorder affects those results.

In what follows, we will first analyze the results of the deterministic model and then the results in presence of disorder. In figures 2, 4, and 5 the results of the deterministic model are shown in the left panels, while those in presence of disorder, are in the right panels.

2.1. Analysis of the deterministic model

According to our previous assumptions, the behavior of the efficiency η in the $(X, \delta E_{\text{rc}})$ -plane depends on the ratio between the two system parameters Δ and V_{rc} . Since it is relevant for natural systems, we first consider the case $\Delta = 0$, which corresponds to two uncoupled ring sites in the trimer model ($\Omega = 0$) equally connected to the RC. In this case, the sole energy scale of the system is V_{rc} . We will subsequently consider the effects of a finite gap $\Delta \neq 0$.

2.1.1. The zero-gap case With $\Delta = 0$ our model corresponds to a tight-binding chain of three sites, the first (subradiant) is coupled via X to the second (superradiant), with equal energy, which is coupled to the RC with strength V_{rc} . It can be easily checked that, if we initially excite the subradiant state, the probability $P_{\text{rc}}(t)$ of finding the excitation on the RC (which is a periodic function of time if we neglect the non-Hermitian terms in (4)) can reach the maximal value of 1 in the shortest time when $X = V_{\text{rc}}$ and $\delta E_{\text{rc}} = 0$,

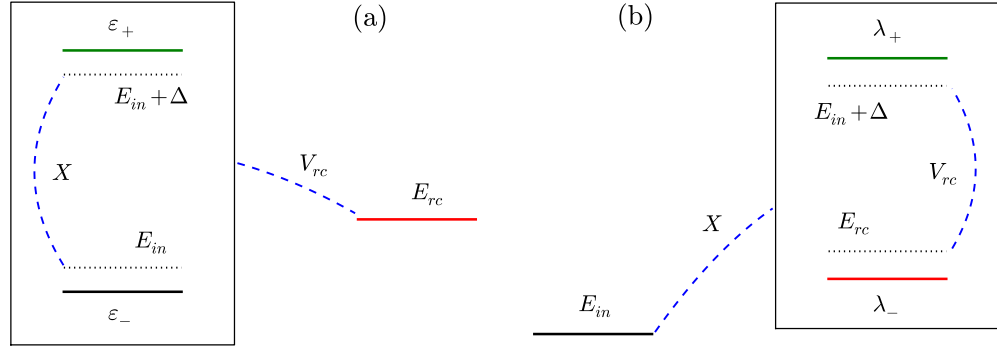


Figure 3. Different schematic representations of the energy levels in the deterministic trimer model. (a) The subradiant-superradiant subsystem (framed), where the coupling X produces the dressed levels with energies ε_{\pm} , is coupled through V_{rc} to the RC state at energy E_{rc} . (b) The initial subradiant state at energy E_{in} is coupled through X to the superradiant-RC subsystem (framed), where the coupling V_{rc} produces the dressed levels with energies λ_{\pm} .

thus identifying the following global optimization condition:

$$X_{\text{opt}} = V_{rc} \quad \text{and} \quad \delta E_{rc}^{\text{opt}} = 0. \quad (5)$$

The estimate given in (5), obtained considering the coherent transfer of excitation between the subradiant and the RC states, is a very good estimate also of the global optimum of the transfer efficiency, as shown in figure 2 (blue cross in left panel).

We observe that the condition $\delta E_{rc} = 0$ is not necessary for the probability of being on the RC to reach 1, but, in combination with $X = V_{rc}$, it makes such transfer the fastest. On the other hand, if we have some constraint on the coupling X enforcing the condition $X \gg V_{rc}$, the optimal detuning is not $\delta E_{rc} = 0$.

To find the resonant detuning producing the optimal transfer in the case $X \gg V_{rc}$ we can consider V_{rc} as a perturbation, obtaining the picture illustrated in panel (a) of figure 3. The subradiant and superradiant states couple and give rise to the dressed energy levels

$$\varepsilon_{\pm}(X) = E_{in} + \frac{\Delta}{2} \pm \sqrt{\frac{\Delta^2}{4} + X^2}, \quad (6)$$

which reduce to $\varepsilon_{\pm}(X) = E_{in} \pm X$ for $\Delta = 0$ (recall that we considered both κ and Γ_{fl} as small perturbations, that can be neglected in finding the dressed energies). The initial excitation is equally distributed on those levels, and we can then identify two optimal detuning values by the symmetric resonant tunneling conditions

$$E_{rc} = \varepsilon_{\pm}(X), \quad (7)$$

entailing

$$\delta E_{rc}(X) = \frac{\Delta}{2} \pm \sqrt{\frac{\Delta^2}{4} + X^2}. \quad (8)$$

For the case $\Delta = 0$ we have $\delta E_{rc}(X) = \pm X$ (see dashed curves in figure 2). Note that in (8) we kept the dependence on Δ , since it will be relevant in the following.

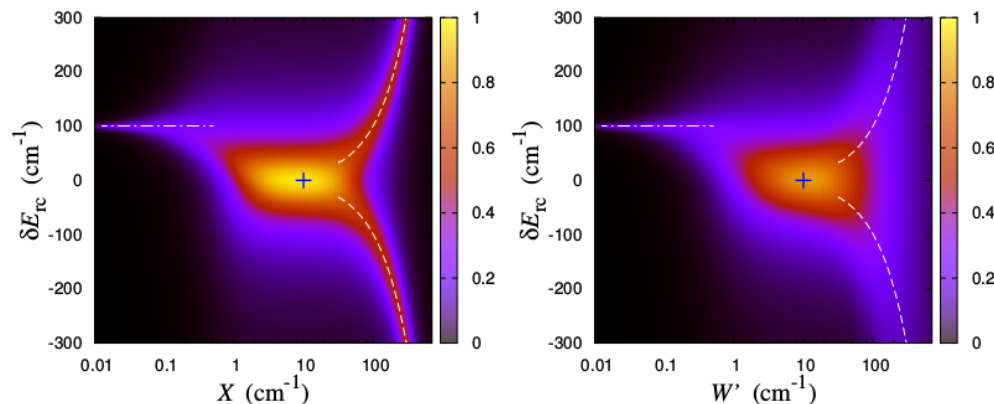


Figure 4. Average transfer efficiency η at fluorescence time $t_{\text{fl}} = \hbar/\Gamma_{\text{fl}}$, computed starting from the subradiant state $|SUB\rangle$, plotted in the left panel as a function of the subradiant-RC detuning δE_{rc} and of the deterministic subradiant-superradiant coupling X , and in the right panel as a function of δE_{rc} and of the rescaled disorder strength $W' = W/\sqrt{2}$. The blue cross indicates the estimate (5) for the optimal transfer conditions. The dashed curves indicate the resonances determined in (8) and the dot-dashed line marks the the resonant condition (11). The value of the parameters are $\Delta = 1 \text{ cm}^{-1}$, $V_{\text{rc}} = 10 \text{ cm}^{-1}$, $\kappa = 0.01 \text{ cm}^{-1}$, and $\Gamma_{\text{fl}} = 10^{-4} \text{ cm}^{-1}$.

2.1.2. The finite-gap case We will now investigate whether the optimal conditions given in equation (5) are valid also for finite values of the energy gap Δ . We will show that condition (5) gives a good estimate for the global optimum whenever V_{rc} is of the same order of Δ in the deterministic model, while disorder produces some modifications, as discussed in the next subsection.

Let us first consider the situation when the energy gap Δ is finite and $\Delta < V_{\text{rc}}$. We see from figure 4 that the global optimization condition (5) (blue cross) is still an excellent estimate for the configuration with maximal efficiency, and also the symmetric resonances present for $X \gg V_{\text{rc}}$ follow the analytic prediction (8) (see dashed curves in figure 4). Nevertheless, figure 4 enlightens a somewhat unexpected feature: if we assume now the coupling X to be constrained within the region $X \ll \Delta < V_{\text{rc}}$, the RC energy producing the maximal efficiency, identified by a sharp resonance, is very far from either E_{in} or ε_{\pm} .

To understand such a resonance, we can now consider X as a small perturbation, exploiting the picture illustrated in panel (b) of figure 3. The superradiant and the RC states couple to give the dressed energy levels

$$\lambda_{\pm}(E_{\text{rc}}) = \frac{1}{2} (E_{\text{in}} + \Delta + E_{\text{rc}}) \pm \sqrt{\frac{1}{4} (E_{\text{in}} + \Delta - E_{\text{rc}})^2 + V_{\text{rc}}^2}, \quad (9)$$

which clearly depend on the RC energy E_{rc} . The initial excitation is all on the subradiant state, since X is small, and a resonant tunneling criterion would now require E_{in} to match the energies λ_{\pm} of the superradiant-RC subsystem. Nevertheless, we have $E_{\text{in}} < E_{\text{in}} + \Delta < \lambda_{+}$ by construction, so that the resonant condition for $X \ll \Delta < V_{\text{rc}}$

must be

$$E_{\text{in}} = \lambda_-(E_{\text{rc}}), \quad (10)$$

entailing

$$\delta E_{\text{rc}} = \frac{V_{\text{rc}}^2}{\Delta}, \quad (11)$$

which corresponds exactly to the numerical results (see dot-dashed line in figure 4).

If we now decrease further the ratio V_{rc}/Δ we find the following remarkable result (see figure 5, left upper panel): the estimate (5), which was obtained for $V_{\text{rc}} \gg \Delta$, still identifies the global efficiency optimization in the deterministic model (blue cross). Moreover, the resonances predicted by (8) for $X \gg V_{\text{rc}}, \Delta$ and by (11) for $X \ll V_{\text{rc}}, \Delta$ still correspond to the local optimization of the efficiency (see white curves in figure 5). As for the model in presence of disorder (right upper panel of figure 5), while the estimate (5) is still within a region of significant efficiency, the optimal condition is modified by disorder, as a more detailed analysis shows (see lower panels of figure 5 and the discussion in the next subsection).

We finally observe that the width in energy δE_{rc} of the high-efficiency region at the optimal value of X is proportional to the coupling V_{rc} , providing a measure of the robustness of transfer to perturbations around the optimal detuning.

2.2. The effect of disorder

As can be clearly seen from figures 2 and 4, where $V_{\text{rc}} \gg \Delta$, the results obtained from the deterministic model are in good agreement with those in presence of disorder. Indeed, we can obtain an excellent estimate for the global optimization condition by simply substituting the deterministic coupling X with $W/\sqrt{2}$ in (5) (blue crosses in figures 2 and 4, right panels).

On the other side, when $V_{\text{rc}} \lesssim \Delta$ (figure 5), disorder induces some modification of the global optimization condition. This effect can be clearly seen by comparing the two lower panels of figure 5, which describe a situation with $V_{\text{rc}}/\Delta \approx 0.5$, similar to the one we will find in the realistic model considered below. By comparing the two lower panels of figure 5, one can see that the average over disorder shifts the optimal detuning from $\delta E_{\text{rc}} = 0$ to the low-disorder resonance $\delta E_{\text{rc}} = V_{\text{rc}}^2/\Delta$ given by (11). This can be explained from the fact that the random coupling falls for many realizations in the region $x < V_{\text{rc}} \lesssim \Delta$, where the resonance is for $\delta E_{\text{rc}} = V_{\text{rc}}^2/\Delta$ and not for $\delta E_{\text{rc}} = 0$. As far as optimal disorder is concerned, even if (5) overestimates its actual value, it still gives an estimate within 5% of the maximal efficiency, see figure 5 lower right panel.

Note that the case $V_{\text{rc}} \ll \Delta$ has not been discussed since it is not relevant for the realistic model considered in the next section.

Summarizing, we predict the global optimization of the average transfer efficiency $\eta(t \gtrsim \hbar/\Gamma_{\text{fl}})$ from the subradiant state of the trimer into the sink placed at the RC as given by

$$W_{\text{opt}}/\sqrt{2} \simeq V_{\text{rc}} \quad \text{and} \quad E_{\text{rc}} = E_{\text{in}} \quad \text{for} \quad V_{\text{rc}} \gg \Delta, \quad (12)$$

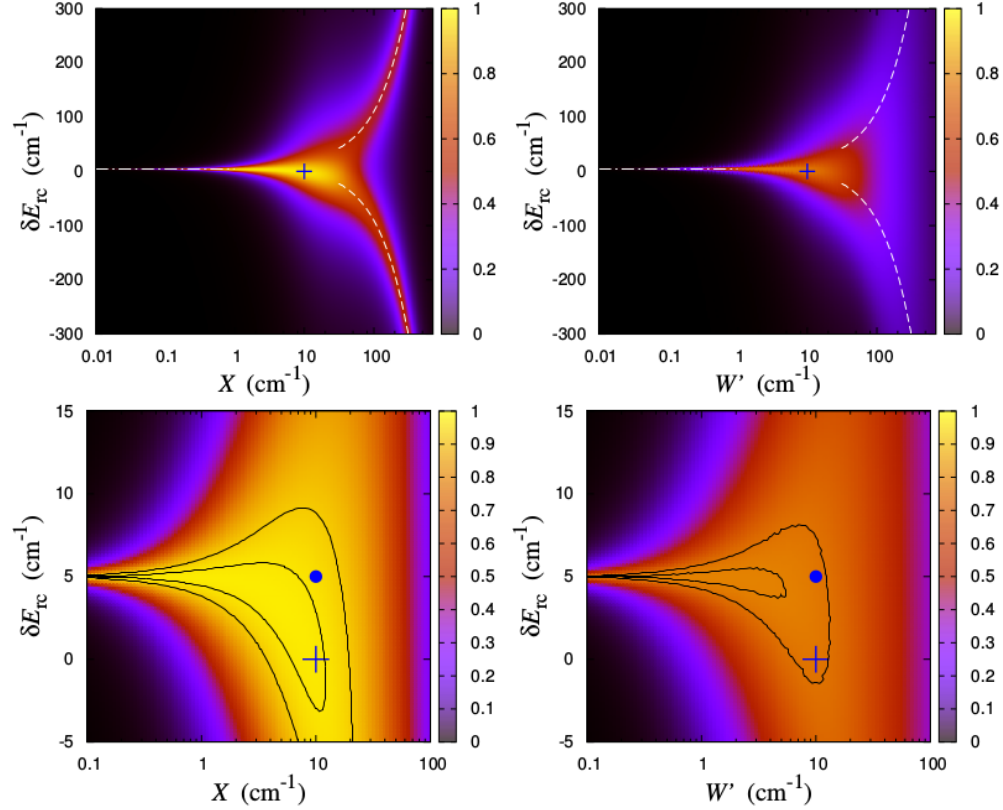


Figure 5. Average transfer efficiency η at fluorescence time $t_{\text{fl}} = \hbar/\Gamma_{\text{fl}}$, computed starting from the subradiant state $|SUB\rangle$, plotted in the left panels as a function of the subradiant-RC detuning δE_{rc} and of the deterministic subradiant-superradiant coupling X , and in the right panels as a function of δE_{rc} and of the rescaled disorder strength $W' = W/\sqrt{2}$. The blue cross indicates the estimate (5) for the optimal transfer conditions. In the upper panels the dashed curves indicate the resonances determined in (8) and the dot-dashed line marks the the resonant condition (11). In the lower panels we zoomed on the high-efficiency regions to show how disorder affects the accuracy of the estimates (5) and (12). The blue dots mark the modification (13) of the estimate proposed in section 2.2. Isolines enclose the regions of efficiency lying within 1% and 5% of the maximal efficiency. The value of the parameters are $\Delta = 20 \text{ cm}^{-1}$, $V_{\text{rc}} = 10 \text{ cm}^{-1}$, $\kappa = 0.01 \text{ cm}^{-1}$, and $\Gamma_{\text{fl}} = 10^{-4} \text{ cm}^{-1}$.

and

$$W_{\text{opt}}/\sqrt{2} \simeq V_{\text{rc}} \quad \text{and} \quad E_{\text{rc}} = E_{\text{in}} + \frac{V_{\text{rc}}^2}{\Delta} \quad \text{for} \quad V_{\text{rc}} \lesssim \Delta. \quad (13)$$

Our results also confirm the expectation that the width in energy δE_{rc} of the high-efficiency region at the optimal disorder strength is proportional to the superradiant coupling V_{rc} .

Another physically relevant question concerns the optimal detuning at some fixed disorder strength determined by physiological conditions (natural systems are usually subject to a definite range of static disorder). In this situation our results indicate that, if the disorder is constrained to be smaller than the energy gap Δ and the coupling V_{rc} ,

the optimal subradiant-RC detuning is not zero, but it is always given by

$$\delta E_{\text{rc}} = \frac{V_{\text{rc}}^2}{\Delta}, \quad (14)$$

with a significant efficiency present only in a narrow band around such optimal detuning. This result is at variance with the intuitive expectation that the best transport would be obtained at resonance with the initial state, $\delta E_{\text{rc}} = 0$. Moreover, it can be easily extended to N -sites rings and its general validity will be the subject of future investigations.

For large values of the disorder, as a result of the averaging procedure, we have a broad resonance centered around $\delta E_{\text{rc}} = 0$, which fades into two very broad resonances centered around $E_{\text{rc}} = \varepsilon_{\pm}(W/\sqrt{2})$ given by condition (7), characterized by a negligible efficiency.

3. Application to natural complexes

Let us analyze a model of the light-harvesting complex I (LHI) and the RC of purple bacteria. Our purpose is to determine the optimal efficiency as a function of both the energy detuning of the RC with respect to LHI and the disorder strength. We will use the previous findings concerning the trimer model to estimate such global optimum.

3.1. LHI-RC complex of purple bacteria

The LHI-RC complex of purple bacteria can display a variety of forms depending on the species (see [32] for a review). To illustrate the relevance of our analysis in such complexes we focus on the model presented in [31]. It consists of 32 chromophores arranged to form the LHI ring with equal energies e_r , plus 4 central chromophores which represent the RC: a special pair with energy e_s (labeled as 33, 34) and two accessory sites with energy e_a (labeled as 35, 36), see figure 6. The chromophores are modeled as two-level systems (sites) and, since in physiological situations the complex is irradiated by a dilute light, we can safely apply the single-excitation approximation. The interaction among sites is due to the transition dipole moments of the chromophores, except for the nearest neighbors where the dipole approximation is no longer valid. We then assume, following [31], such interaction strength to take the values Ω_1, Ω_2 alternating each site, which can be determined by fitting the energy spectrum of the LHI complex. Moreover, the two inner sites of the RC with energy e_s have also a short-range coupling Ω_{sp} determined in a similar way.

For positions \vec{R}_s and orientations $\vec{\mu}_s$ of the dipole moments as well as for the nearest neighbor interactions $(\Omega_1, \Omega_2, \Omega_{\text{sp}})$ and the site energies (e_r, e_s, e_a) we took the data (reported in Table A1 and Table A2 in the Appendix) from [31].

The Hamiltonian of the system, written on the site-basis $|s\rangle$, $s = 1, \dots, 36$, reads

$$H_{\text{rhod}} = e_r \sum_{s=1}^{32} |s\rangle \langle s| + e_s \sum_{s=33}^{34} |s\rangle \langle s| + e_a \sum_{s=35}^{36} |s\rangle \langle s|$$

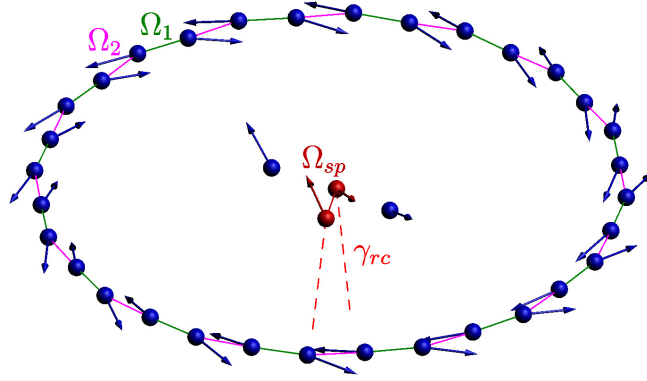


Figure 6. Spatial structure of the LHI-RC complex. The two red sites are the special pair (33, 34) (“open” sites) from which the excitation can escape. The other two sites in the center are part of the RC, but they are “closed”, in the sense that they contribute to the interaction with the other sites but the excitation can not escape from them. The arrows indicate the directions of the dipole moments.

$$\begin{aligned}
& + \Omega_1 \sum_{s=1}^{16} (|2s-1\rangle \langle 2s| + |2s\rangle \langle 2s-1|) \\
& + \Omega_2 \sum_{s=1}^{15} (|2s\rangle \langle 2s+1| + |2s+1\rangle \langle 2s|) \\
& + \Omega_2 (|32\rangle \langle 1| + |1\rangle \langle 32|) + \Omega_{sp} (|33\rangle \langle 34| + |34\rangle \langle 33|) \\
& + C \widehat{\sum_{s,r}} \left[\frac{\vec{\mu}_s \cdot \vec{\mu}_r}{R_{sr}^3} - \frac{3(\vec{R}_{sr} \cdot \vec{\mu}_s)(\vec{R}_{sr} \cdot \vec{\mu}_r)}{R_{sr}^5} \right], \tag{15}
\end{aligned}$$

where \vec{R}_{sr} is the vector connecting the site s to r , $\vec{\mu}_s$ is the dipole moment at the site s , and the constant C embeds the dipole strength common to all of the chromophores. The hat over the last summation indicates that we consider the interaction among all sites (ring and RC) but the terms associated with nearest neighbors along the ring and the special pair.

The loss of excitation into the RC is modeled by two independent sinks attached only to the sites of the special pair (33, 34) with identical decay widths γ_{rc} . Hence, the effective non-Hermitian Hamiltonian for the system is

$$H = H_{\text{rhod}} - i \frac{\gamma_{rc}}{2} \sum_{s=33}^{34} |s\rangle \langle s|. \tag{16}$$

The geometry of the system is illustrated in figure 6 and we want to stress the fact that, while a symmetry of LHI under cyclic permutations of *dimers* can be devised, the geometry of RC sites has no symmetry whatsoever.

Even in this realistic complex it is possible to identify LHI states that are superradiant/subradiant with respect to the transfer of excitation towards the RC states, where the excitation can be trapped. To this end, we first perform two independent

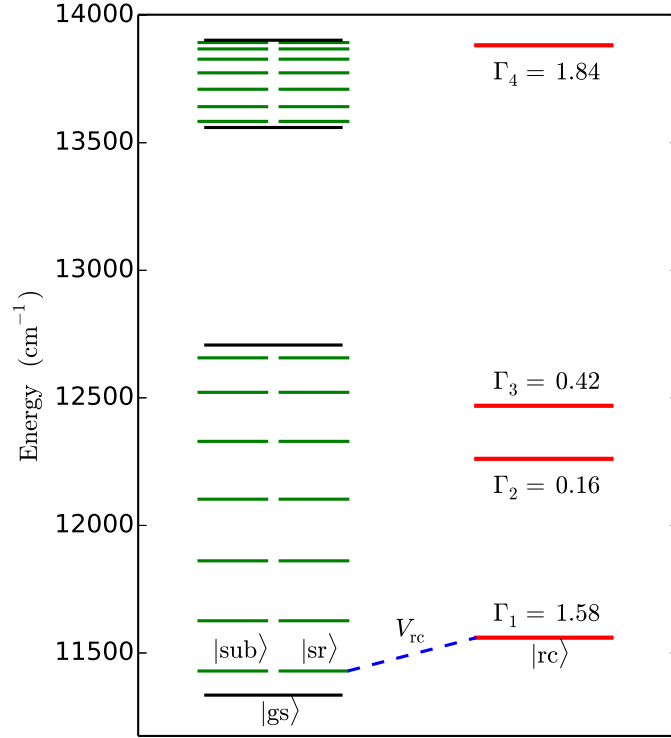


Figure 7. Schematic representation of the 32 energy levels of the LHI complex (left) and of energies and decay widths, in cm^{-1} , of the four RC eigenstates (right) of purple bacteria.

diagonalizations of the LHI and RC sectors of the total Hamiltonian. Since the LHI sector of H is Hermitian, it can be diagonalized by means of a real orthogonal matrix R^{LHI} (which is unitary), while the RC sector, being a non-Hermitian symmetric matrix, is diagonalized by a complex orthogonal matrix R^{RC} (which is non-unitary). By performing the transformation $(R^{\text{LHI}} \otimes R^{\text{RC}})^t H (R^{\text{LHI}} \otimes R^{\text{RC}})$, the total Hamiltonian takes the form

$$\begin{pmatrix} \text{diag}(E_i^{\text{LHI}}) & \vec{a} & \vec{b} & \vec{c} & \vec{d} \\ \vec{a}^t & \mathcal{E}_1^{\text{RC}} & 0 & 0 & 0 \\ \vec{b}^t & 0 & \mathcal{E}_2^{\text{RC}} & 0 & 0 \\ \vec{c}^t & 0 & 0 & \mathcal{E}_3^{\text{RC}} & 0 \\ \vec{d}^t & 0 & 0 & 0 & \mathcal{E}_4^{\text{RC}} \end{pmatrix}$$

where $E_1^{\text{LHI}} \leq E_2^{\text{LHI}} \leq \dots E_{32}^{\text{LHI}}$, are the (real) energy levels of the LHI system and

$$\mathcal{E}_k^{\text{RC}} = E_k^{\text{RC}} - \frac{i}{2}\Gamma_k, \quad k = 1, \dots, 4,$$

are the complex eigenvalues of the RC system, with energy E_k^{RC} and decay width Γ_k . The vectors \vec{a} , \vec{b} , \vec{c} , and \vec{d} represent the coupling between the LHI eigenstates and the RC eigenstates. The intensity of such couplings ranges typically from 0 to 50 cm^{-1} , with average intensity of about 6 cm^{-1} . The energy levels of the LHI-RC system thus obtained are illustrated in figure 7.

By analyzing the coupling vectors \vec{a} , \vec{b} , \vec{c} , and \vec{d} , we can observe that, due to the peculiar symmetry structure of the system at hand, there is a great inhomogeneity in their intensity. Indeed, for any RC level we can identify a set of superradiant LHI states (strongly coupled) and a set of subradiant LHI states (weakly coupled). Such a distinction will be important in making the transport properties amenable to an analysis based on the trimer model discussed in section 2.

The effect of the static disorder has been taken into account by adding to H the disorder Hamiltonian

$$D = \sum_{s=1}^{36} \delta_s |s\rangle \langle s|, \quad (17)$$

where the δ_s 's are independent Gaussian random variables centered in 0 and with variance W^2 . The disorder will produce a random coupling between subradiant and superradiant states with variance $\sim W^2/N$, where $N = 32$ is the number of LHI sites. Indeed, the diagonalization of the LHI sector of (17) produces a $N \times N$ full random matrix with Gaussian entries centered in 0 and with variance $\sim W^2/N$, whereas the diagonalization of the RC sector (which has 4 sites) produces a 4×4 full random matrix with Gaussian entries centered in 0 and with variance $\sim W^2/4$.

It should be noted that the value e_r of the LHI site energy can be nicely determined by fitting the absorption spectra of the LHI complex, whereas the RC energies e_s and e_a are reported to be lower than e_r , but their precise value is not well known and they can be shifted to match other experimental findings such as the high values of efficiency (see the discussion in [31]).

The coupling with the electromagnetic field, which induces superabsorption and superfluorescence of light, has been taken into account adding to the Hamiltonian in (16) a non-Hermitian part, following the procedure described in [10].

In the following we will keep all the parameters of the model fixed, except for the RC energies and the strength W of the disorder, with the aim to find the global optimum. To achieve this goal, we will show how the main features of the transport properties of the LHI-RC complex are obtained by reducing it to two independent trimers.

3.2. Reduction procedure

In this complex we have many LHI states coupled to four RC energy levels, so that it may seem very difficult to optimize the transfer efficiency by choosing the RC energies and the disorder strength independently of the LHI state initially excited. Nevertheless, in physiological conditions the ground state and the first two degenerate excited states of the LHI ring are the most populated ones (together they gather 77% of the total probability at $T = 288$ K). Moreover, the only state of the RC we need to consider is the lowest energy state, since the other three RC states are separated from it by a significant energy gap, which makes their effective coupling to the most populated LHI states negligible.

In the doubly degenerate subspace of the first two excited LHI states, if we consider the coupling to the RC, it is possible to identify a subradiant state and a superradiant one, denoted by $|\text{sub}\rangle$ and $|\text{sr}\rangle$, respectively (see figure 7). Those states are such that

$$\langle \text{sub} | H | \text{rc} \rangle = a_2 = 0, \text{ and } \langle \text{sr} | H | \text{rc} \rangle = a_3 = -43.71 \text{ cm}^{-1}.$$

Moreover, the LHI ground state $|\text{gs}\rangle$ is subradiant with respect to transfer towards $|\text{rc}\rangle$, since the coupling intensity

$$|\langle \text{gs} | H | \text{rc} \rangle| = |a_1| = 0.26 \text{ cm}^{-1}$$

is much smaller than the average coupling, and negligible if compared to $|a_3| = 43.71 \text{ cm}^{-1}$.

As already noted, we view the energy value E_1^{RC} of $|\text{rc}\rangle$ as an adjustable parameter, which can be modified by shifting all of the RC energies e_s, e_a of the same amount. Note that the first two excited states are optically very active [31], concentrating most of the LHI fluorescence, while the $|\text{gs}\rangle$ is optically almost inactive. On the other hand, the transfer from $|\text{sr}\rangle$ towards the RC is very fast, due to its strong coupling. It is then capable to compete with (and outperform) the decay due to fluorescence. Moreover, when the coupling between $|\text{sub}\rangle$ and $|\text{sr}\rangle$ induced by disorder is strong enough, also the transfer from $|\text{sub}\rangle$ becomes significant. For this reason, in our numerical simulations of the LHI-RC complex we took into account fluorescence in an exact way, following the approach presented in [10]. Such approach includes the effect of superradiant loss of excitation into the electromagnetic field, thus allowing to estimate the competition between superradiant loss and superradiant transfer of the excitation.

The problem of excitation transfer from an initial Gibbs populations distributed on the three lowest-energy levels towards the lowest RC energy can be decomposed in two independent problems, involving two trimers: (A) LHI ground state $|\text{gs}\rangle$, superradiant $|\text{sr}\rangle$, and $|\text{rc}\rangle$; (B) subradiant excited state $|\text{sub}\rangle$, superradiant $|\text{sr}\rangle$, and $|\text{rc}\rangle$.

Concerning the trimer A, we neglect the direct coupling a_1 since it is much weaker than a_3 , and we use the model Hamiltonian (4) with the identifications

$$\Delta = E_3^{\text{LHI}} - E_1^{\text{LHI}} = 94 \text{ cm}^{-1} \text{ and } V_{\text{rc}} = |a_3| = 43.71 \text{ cm}^{-1}.$$

As for trimer B, we can use again the model Hamiltonian (4) with $\Delta \simeq 0$, since

$$E_2^{\text{LHI}} = E_3^{\text{LHI}} = 11429 \text{ cm}^{-1},$$

and $V_{\text{rc}} = |a_3|$. In both models the opening strength κ in (4) is given by $\Gamma_1 = 1.58 \text{ cm}^{-1}$. Moreover, the variance of the random coupling between subradiant states and $|\text{sr}\rangle$, which will be important in what follows, is of the order of W^2/N (with $N = 32$).

3.3. Optimality conditions

At room temperature the excitation is evenly shared among the states $|\text{gs}\rangle$ (33%), $|\text{sub}\rangle$ (22%) and $|\text{sr}\rangle$ (22%). To find the optimal conditions we will focus on the subradiant states, which are the only ones to display a non-monotone behavior with disorder. Moreover, we can use the conditions found in section 2 for the trimer model.

Transfer from $|\text{gs}\rangle$. Given that $|a_1| \ll |a_3|$, the indirect connection between $|\text{gs}\rangle$ and $|\text{rc}\rangle$ through $|\text{sr}\rangle$ is the most relevant. We then expect that, to find the optimal value of E_1^{RC} relative to transfer from $|\text{gs}\rangle$, one must consider the trimer A, which predicts the optimal resonant configuration at

$$E_1^{\text{RC}} = E_{\text{res}}^{\text{gs}} = E_1^{\text{LHI}} + \frac{|a_3|^2}{E_3^{\text{LHI}} - E_1^{\text{LHI}}} \approx 11355 \text{ cm}^{-1},$$

since $V_{\text{rc}}/\Delta \approx 0.5$ (see conditions (13)). Such a configuration can be produced by setting the energy of the special pair $e_s = E_1^{\text{RC}} + 1188 \text{ cm}^{-1} = 12543 \text{ cm}^{-1}$. The robustness with respect to detuning of such optimum has been discussed in section 2, indicating that E_1^{RC} should lie within an interval $\pm V_{\text{rc}}$ around $E_{\text{res}}^{\text{gs}}$. As explained in section 2, the optimal disorder is given by the condition $\sigma_{\text{gs}} \simeq W/\sqrt{N} \simeq V_{\text{rc}} = |a_3|$, which produces the estimate $W_{\text{opt}} \simeq 250 \text{ cm}^{-1}$. The optimal transfer conditions for trimer A are then:

$$W \simeq 250 \text{ cm}^{-1} \quad \text{and} \quad E_1^{\text{RC}} = E_{\text{res}}^{\text{gs}} \pm V_{\text{rc}} \simeq (11355 \pm 44) \text{ cm}^{-1}.$$

Transfer from $|\text{sub}\rangle$. In this case ($\Delta = 0$) the optimal detuning is zero (see conditions (12)), entailing $E_1^{\text{RC}} = E_3^{\text{LHI}} \pm V_{\text{rc}}$, and the optimal disorder is again given by $\sigma_{\text{sub}} \simeq W/\sqrt{N} \simeq V_{\text{rc}}$. So that the optimal conditions for this case are

$$W \simeq 250 \text{ cm}^{-1} \quad \text{and} \quad E_1^{\text{RC}} = E_{\text{res}}^{\text{gs}} \pm V_{\text{rc}} \simeq (11429 \pm 44) \text{ cm}^{-1}.$$

Global conditions. From the discussion above we see that the global optimization conditions are somewhat different for each of the two LHI states we analyzed, but the cooperatively enhanced superradiant coupling V_{rc} is large enough to allow for a significant overlap of the high-efficiency regions pertaining to each initial state. This overlap identifies the interval

$$E_1^{\text{RC}} \simeq (11392 \pm 7) \text{ cm}^{-1}, \tag{18}$$

corresponding to $e_s = (12580 \pm 7) \text{ cm}^{-1}$. On the other side, from the above discussion it is clear that the optimal disorder range is $W \simeq 250 \text{ cm}^{-1}$.

This estimate of the global optimal conditions is shown as a blue cross in figure 8 and it is very close to the region of maximal efficiency found numerically. Note that, while the detuning energy is in excellent agreement with the numerical results, the optimal disorder slightly overestimates the actual maximal value. This can be due to the fact that the efficiency of the superradiant state (not considered here) decreases with disorder, thus producing a lowering of the optimal disorder value. Another possible cause of deviation might be that for the ground state the optimal disorder can be lower than what we estimated, as emerges from the discussion about figure 5, lower right panel. Note that the optimal disorder strength falls within the range of the natural disorder strengths (30 cm^{-1} to 300 cm^{-1} [23, 12]).

The results presented in figure 8 also show that, for small disorder strength, the transfer of excitation from the LHI ring into the RC has an optimal efficiency when $E_1^{\text{RC}} = E_{\text{res}}^{\text{gs}}$ (horizontal dot-dashed line), consistent with our analysis, whereas both the

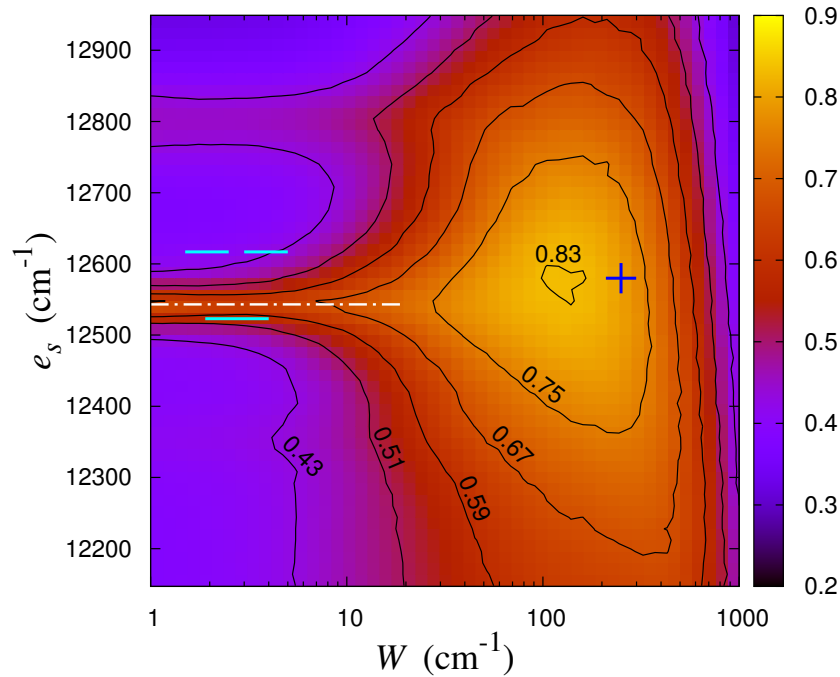


Figure 8. Average transfer efficiency at 20 ns for the LHI-RC complex, starting from a Gibbs distribution of LHI eigenstates at temperature $T = 288$ K, plotted as a function of the disorder strength W and of the energy e_s of the special pair. The horizontal dot-dashed line indicates the value of $e_s = 12543$ cm^{-1} for which $E_1^{\text{RC}} = E_{\text{res}}^{\text{gs}}$ (resonant configuration). The blue cross marks the estimated optimal conditions, see text. The values of e_s such that $E_1^{\text{RC}} = E_j^{\text{LHI}}$, $j = 1, 2, 3$, (possible resonances with the first three LHI eigenstates) are marked with cyan bars.

configurations with $E_1^{\text{RC}} = E_1^{\text{LHI}}$ or $E_1^{\text{RC}} = E_2^{\text{LHI}} = E_3^{\text{LHI}}$ (marked with cyan bars in figure 8) would produce a lower efficiency for small W . Note that we computed the transfer efficiency at $t = 20$ ns, a time larger than the average fluorescence time.

4. Conclusions

We considered both paradigmatic and realistic models of quantum networks in which a ring of peripheral sites is coupled to some inner sites, where the excitation can be trapped in a reaction center. In similar networks the ring states can often be classified as superradiant or subradiant, based on how they transfer the excitation into the reaction center.

Subradiant states are not directly coupled to the reaction center, but static on-site disorder can effectively couple them with superradiant states. This opens an indirect path for the transfer of excitation from subradiant states to the reaction center mediated by the superradiant state. The static disorder which activates the transfer from subradiant states, when too strong, hinders transport so that an optimal disorder condition can be determined.

We identify the building block of such kind of transport: a trimer with a subradiant

initial state, a target RC state, and a superradiant state coupled to the RC and, via static disorder, to the subradiant state. Four parameters determine the different regimes in which the trimer can operate: the energy distance Δ between the subradiant and the superradiant state, the intensity W of the random coupling between those states, the direct coupling V_{rc} between the superradiant state and the RC, and the detuning δE_{rc} between the subradiant initial state and the RC.

We study how to optimize the energy transfer efficiency by varying both the disorder strength W and the detuning δE_{rc} . We determine such optimal conditions as given by: (i) $W \simeq V_{\text{rc}}$ and $\delta E_{\text{rc}} = 0$ for $V_{\text{rc}} \gg \Delta$; (ii) $W \simeq V_{\text{rc}}$ and $\delta E_{\text{rc}} = V_{\text{rc}}^2/\Delta$ for $V_{\text{rc}} \lesssim \Delta$. Note that the optimal disorder is determined by the superradiant coupling V_{rc} . We also discuss how to determine the optimal detuning when the disorder strength is constrained to be much smaller or much larger than both Δ and V_{rc} .

Notably, our general results can be applied to a realistic model for the light-harvesting complex (LHI) and reaction center (RC) of purple bacteria. A reduction of the whole systems to a set of independent trimers allows for a detailed explanation of the whole process of transfer from an initial Gibbs thermal state and justifies the very high efficiency of excitation transfer even at room temperature. Our analysis points towards a possible correlation between the structure of such a system and transfer optimization. Indeed, the superradiant coupling generated by the symmetry of the LHI complex is strong enough to allow for a simultaneous optimization of transfer from the relevant LHI eigenstates. Moreover, it entails an optimal disorder strength for the transfer from such Gibbs distribution of initial states that falls within the estimated range of physiological disorder. We believe that our analysis covers those quantum networks in which a subradiant subspace (also known in literature as trapping-free subspace [6]) is present. Especially to understand the enhancement in transport due to disorder, which is ubiquitous in such structures, it is necessary to go beyond the standard perturbative analysis.

It will be important to consider, in a future work, the effect of different baths, represented by noise with short correlation time, which induce loss of coherence during the quantum evolution. Indeed, the different nature of such kind of noise, always present in physiological situations, and their interplay with static disorder may entail different estimates for the optimal noise strength, while we expect the resonant tunneling criterion to remain as presented in this paper.

Acknowledgments

This work was partially supported by the research promotion initiative of Università Cattolica del Sacro Cuore. We also acknowledge useful discussions with Lev Kaplan, Debora Contreras-Pulido, and Robin Kaiser.

Table A1. Energy and coupling parameters of the model for the LHI-RC complex.

Description	Symbol	Value
energy of the ring sites	e_r	12911 cm^{-1}
energy of the special pair (33, 34)	e_s	12748 cm^{-1}
energy of the accessory pair (35, 36)	e_a	12338 cm^{-1}
coupling within a dimer ($2s + 1, 2s$)	Ω_1	806 cm^{-1}
coupling across two dimers ($2s, 2s + 1$)	Ω_2	377 cm^{-1}
coupling within the special pair (33, 34)	Ω_{sp}	1000 cm^{-1}
dipole strength of all of the chromophores	C	$519310 \text{ \AA}^3 \text{ cm}^{-1}$

Appendix A. Data for the realistic model

The values of the parameters entering the definition of Hamiltonian (15) for the realistic model of the LHI-RC complex of the purple bacterium *Rhodobacter Sphaeroides* have been taken from [31] and are reported in Tables A1 and A2.

References

- [1] Engel G S, Calhoun T R, Read E L, Ahn T K, Mancal T, Cheng Y C, Blankenship R E and Fleming G R 2007 *Nature* **446** 782–786; Panitchayangkoon G, Hayes D, Fransted K A, Caram J R, Harel E, Wen J Z, Blankenship R E and Engel G S 2010 *Proc. Nat. Acad. Sci. Am.* **107** 12766–12770; Collini E, Wong C, Wilk K, Curmi P, Brumer P and Scholes G 2010 *Nature* **463** 644–649
- [2] Celardo G L, Borgonovi F, Tsifrinovich V I, Merkli M and Berman G P 2012 *J. Phys. Chem. C* **116** 22105
- [3] Ferrari D, Celardo G L, Berman G P, Sayre R T and Borgonovi F 2014 *J. Phys. Chem. C* **118** 20
- [4] Lloyd S and Mohseni M 2010 *New J. Phys.* **12** 075020; Scholes G D 2002 *Chem. Phys.* **275** 373
- [5] Anderson P W 1958 *Phys. Rev.* **109** 1492
- [6] Caruso F, Chin A W, Datta A, Huelga S F and Plenio M B 2009 *J. Chem. Phys.* **131** 105106
- [7] Sokolov V V and Zelevinsky V G 1989 *Nucl. Phys.* **A504** 562; Sokolov V V and Zelevinsky V G 1988 *Phys. Lett. B* **202** 10; Rotter I 1991 *Rep. Prog. Phys.* **54** 635; Sokolov V V and Zelevinsky V G 1992 *Ann. Phys. (N.Y.)* **216** 323
- [8] Sadreev A F and Rotter I 2003 *J. Phys. A* **36** 11413; Weiss M, Méndez-Bermúdez J A and Kottos T 2006 *Phys. Rev. B* **73** 045103
- [9] Celardo G L, Izrailev F M, Zelevinsky V G and Berman G P 2008 *Phys. Lett B* **659** 170; Celardo G L, Izrailev F M, Zelevinsky V G and Berman G P 2007 *Phys. Rev. E* **76** 031119.
- [10] Grad J, Hernandez G and Mukamel S 1988 *Phys. Rev. A* **37** 3835; Spano F C, Kuklinski J R and Mukamel S 1991 *J. Chem. Phys.* **94** 7534
- [11] Akkermans E, Gero A and Kaiser R 2008 *Phys. Rev. Lett.* **101** 103602; Kaiser R 2009 *J. Mod. Opt.* **56** 2082; Bienaime T, Piovela N and Kaiser R 2012 *Phys. Rev. Lett.* **108** 123602; Akkermans E and Gero A 2013 *Europhys. Lett.* **101** 54003; Kaiser R 2012 *Nature Physics* **8** 363
- [12] Monshouwer R, Abrahamsson M, van Mourik F and van Grondelle R 1997 *J. Phys. Chem. B* **101** 7241
- [13] Celardo G L and Kaplan L 2009 *Phys. Rev. B* **79** 155108; Celardo G L, Smith A M, Sorathia S, Zelevinsky V G, Sen'kov R A and Kaplan L 2010 *Phys. Rev. B* **82** 165437
- [14] Celardo G L, Biella A, Kaplan L and Borgonovi F 2013 *Fortschr. Phys.* **61** 250–260; Biella A, Borgonovi F, Kaiser R and Celardo G L 2013 *Europhys. Lett.* **103** 57009

Table A2. Position and transition-dipole direction of the LHI-RC sites.

Site	x (Å)	y (Å)	z (Å)	μ_x	μ_y	μ_z
1	44.706	-12.591	71.986	0.634	0.760	0.147
2	47.167	-3.677	72.184	-0.452	-0.886	0.098
3	46.122	5.475	71.986	0.295	0.944	0.147
4	44.984	14.653	72.184	-0.079	-0.992	0.098
5	40.515	22.709	71.986	-0.089	0.985	0.147
6	35.952	30.752	72.184	0.307	-0.947	0.098
7	28.741	36.485	71.986	-0.459	0.876	0.147
8	21.448	42.169	72.184	0.646	-0.757	0.098
9	12.591	44.706	71.986	-0.760	0.634	0.147
10	3.677	47.167	72.184	0.886	-0.452	0.098
11	-5.475	46.122	71.986	-0.944	0.295	0.147
12	-14.653	44.984	72.184	0.992	-0.079	0.098
13	-22.709	40.515	71.986	-0.985	-0.089	0.147
14	-30.752	35.952	72.184	0.947	0.307	0.098
15	-36.485	28.741	71.986	-0.876	-0.459	0.147
16	-42.169	21.448	72.184	0.757	0.646	0.098
17	-44.706	12.591	71.986	-0.634	-0.760	0.147
18	-47.167	3.677	72.184	0.452	0.886	0.098
19	-46.122	-5.475	71.986	-0.295	-0.944	0.147
20	-44.984	-14.653	72.184	0.079	0.992	0.098
21	-40.515	-22.709	71.986	0.089	-0.985	0.147
22	-35.952	-30.752	72.184	-0.307	0.947	0.098
23	-28.741	-36.485	71.986	0.459	-0.876	0.147
24	-21.448	-42.169	72.184	-0.646	0.757	0.098
25	-12.591	-44.706	71.986	0.760	-0.634	0.147
26	-3.677	-47.167	72.184	-0.886	0.452	0.098
27	5.475	-46.122	71.986	0.944	-0.295	0.147
28	14.653	-44.984	72.184	-0.992	0.079	0.098
29	22.709	-40.515	71.986	0.985	0.089	0.147
30	30.752	-35.952	72.184	-0.947	-0.307	0.098
31	36.485	-28.741	71.986	0.876	0.459	0.147
32	42.169	-21.448	72.184	-0.757	-0.646	0.098
33	-3.402	-2.049	68.512	-0.379	-0.860	-0.342
34	3.317	2.301	68.262	0.371	0.871	-0.321
35	3.369	-9.909	72.059	0.208	0.854	-0.476
36	-2.852	10.539	70.886	-0.300	-0.870	-0.391

- [15] Celardo G L, Giusteri G G and Borgonovi F 2014 *Phys. Rev. B* **90** 075113
- [16] Celardo G L, Poli P, Lussardi L and Borgonovi F 2014 *Phys. Rev. B* **90** 085142
- [17] Scully M O and Svidzinsky A A 2010 *Science* **328** 1239
- [18] Cao J S and Silbey R J 2009 *J. Phys. Chem. A* **113** 13825
- [19] Mohseni M, Rebentrost P, Lloyd S and Aspuru-Guzik A 2008 *J. Chem. Phys.* **129** 174106
- [20] Plenio M B and Huelga S F 2008 *New J. Phys.* **10** 113019
- [21] Moix J M, Khasin M and Cao J S 2013 *New. J. Phys.* **15** 085010
- [22] Sener M K and Schulten K 2002 *Phys. Rev. E* **65** 031916; Dempster S E, Jang S and Silbey R J

- 2001 *J. Chem. Phys.* **114** 10015; Sener M k, Lu D, Ritz T, Park S, Fromme P and Schulten K
2002 *J. Phys. Chem. B* **106** 7948–7960; Pelzer K M, Griffin G B, Gray S K and Engel G S 2012
J. Chem. Phys. **136** 164508; Moix J M, Zhao Y and Cao J S 2012 *Phys. Rev. B* **85** 115412
- [23] Olaya-Castro A, Lee C F, Fassioli Olsen F and Johnson N F 2008 *Phys. Rev. B* **78** 085115
- [24] Gaab K and Bardeen C 2004 *J. Chem. Phys.* **121** 7813
- [25] Vlaming S M, Malyshev V A and Knoester J 2007 *J. Chem. Phys.* **127** 154719
- [26] Rebentrost P, Mohseni M, Kassal I, Lloyd S and Aspuru-Guzik A 2009 *New J. Phys.* **11** 033003
- [27] Wu J L, Liu F, Shen Y, Cao J S and Silbey R J 2010 *New J. Phys.* **12** 105012
- [28] Chin A W, Datta A, Caruso F, Huelga S F and Plenio M B 2010 *New J. Phys.* **12** 065002
- [29] Chin A W, Huelga S F and Plenio M B 2012 *Phil. Trans. R. Soc. A* **370** 3638
- [30] Wu J, Silbey R J and Cao J S 2013 *Phys. Rev. Lett.* **110** 200402
- [31] Hu X, Ritz T, Damjanovic A and Schulten K 1997 *J. Phys. Chem. B* **101** 3854; Hu X and Schulten K 1998 *Biophys. J.* **75** 683
- [32] Cogdell R J, Gall A and Köhler J 2006 *Q. Rev. Biophys.* **39** 227–324